coatings

MDPI

*Article*

# A New Process of Chemical Plating Ni-P Electromagnetic Induction Heating Activation on the Surface of Aluminium Alloy Base Material

**Jin Gao †, Kaifang Cui *,†, Siqi Li †, Liang Zhong, Jingxiong Dai, Zhigang Yang and Rongming Qiang**

The School of Manufacturing Science and Engineering, Southwest University of Science and Technology, Mianyang 621000, China; gaojin@mails.swust.edu.cn (J.G.); lisiqi@swust.edu.cn (S.L.); zhongliang@swust.edu.cn (L.Z.); daijingxiong@swust.edu.cn (J.D.); zhgyang@swust.edu.cn (Z.Y.); qiangrongming@mails.swust.edu.cn (R.Q.)

* Correspondence: cuikaifang@swust.edu.cn

† These authors contributed equally to this work.

**Abstract:** Nowadays, there are many surface treatment methods for aluminium alloys; the most commonly used of these is the chemical dip galvanizing process, which is complicated due to its use of large quantities of corrosive drugs. In order to simplify the process, this paper proposes a new electromagnetic induction heating activation method instead of the zinc dipping process. The method works as follows: The substrate is first degreased and then activated. The activation process starts by soaking the degreased substrate in an activation solution, taking it out after ten minutes, and placing it into an induction heating unit. The activation solution is sprayed onto the surface of the substrate while heating, using the energy generated by high temperatures to complete the activation reaction. The surface of the activated substrate forms a nanoscale film of nickel, which is finally utilised as a catalytic centre for ENP (an advanced surface treatment process that deposits a very uniform layer). The optimisation of important parameters of the non-destructive activation process was determined using the L9 Taguchi method. The main parameters ranged from 0.15 L/min to 0.25 L/min for spray rate, 200 °C to 400 °C for heat treatment temperature, and 1:4, 1:5, and 1:6 for $Ni^{2+}$ and $H_2PO_4^-$ ion concentration ratios. The above data were derived from a single variable and were analysed using Minitab 20 software. Scanning electron microscopy (SEM), X-ray photoelectron spectroscopy (XPS), energy spectrometry (EDS), and ultrasonic experiments were used to characterize and analyse the surface morphology, composition, and bond strength of the coatings. The results show that the nanoscale nickel particles can completely cover the surface of the substrate, forming a layer of nano-film. After activation and ultrasonic cleaning for 30 s at an ultrasonic frequency of 40 KHz and a power of 80 W, the surface nano-film was not destroyed, which proves that it had a high bonding strength. After the application of the plating, the plated surface had a compact microstructure, and the continuity was good. Therefore, compared with the currently commonly used zinc dipping process, this process has the advantages of being a low-cost, simple operation, and non-destructive and environmentally friendly activation process for the substrate.

**Keywords:** electroless nickel plating; aluminium alloys; electromagnetic induction heating; activation; environmental protection

check for updates

**Citation:** Gao, J.; Cui, K.; Li, S.; Zhong, L.; Dai, J.; Yang, Z.; Qiang, R. A New Process of Chemical Plating Ni-P Electromagnetic Induction Heating Activation on the Surface of Aluminium Alloy Base Material. *Coatings* **2024**, *14*, 1221. https://doi.org/10.3390/coatings14091221

Academic Editor: Rafael Comesaña

Received: 11 August 2024
Revised: 4 September 2024
Accepted: 14 September 2024
Published: 22 September 2024

**Copyright:** © 2024 by the authors. Licensee MDPI, Basel, Switzerland. This article is an open access article distributed under the terms and conditions of the Creative Commons Attribution (CC BY) license (https://creativecommons.org/licenses/by/4.0/).

## 1. Introduction

Aluminium and aluminium alloys are some of the most widely used metallic materials and are commonly used in the manufacture of aerospace, large ships, and other important devices [1]. With the development of the manufacturing industry, the properties of the aluminium alloy itself can no longer satisfy application under different environmental conditions; for example, in special environments, aluminium alloys cannot satisfy both

hardness and corrosion resistance conditions. Thus, to further improve the performance of aluminium alloys, an appropriate surface treatment should be carried out [2,3].

The current treatment processes to enhance the surface properties of materials include electroplating, chemical plating, micro-arc oxidation, spraying organic coatings, etc. [4–8]. Specific treatment processes need to be selected on a case-by-case basis; among them, chemical plating is a convenient, environmentally friendly, and low-cost surface treatment process. The prepared plating layer is very homogeneous and has a very similar morphology to the substrate, so it is widely used in industrial production [9–14]. Chemical plating, also known as autocatalytic plating without applied current, reduces metal ions in the plating solution to metal monomers with the help of an appropriate amount of reducing agent and deposits them on the surface of the component [15,16]. A Ni-P layer is widely used in chemical plating because of its good toughness, corrosion resistance, decorative properties, etc. However, due to the high surface activity of aluminium alloys, the naturally occurring oxidized film on its surface limits the effect of the chemical nickel-plating treatment. To address this, the commonly used treatment method is a zinc dip pretreatment, which requires the use of large quantities of corrosive chemicals to remove the oxide layer, followed by a zinc dip treatment, using the generated zinc to replace the oxide film on the aluminium alloy, which is conducive to improving the bonding strength and uniformity of the chemically plated coating [17–20]. However, this method has the following problems: the aluminium alloy substrate is dissolved in the alkaline concentrated zincate solution; in the process of zinc dipping treatment, a large number of corrosive drugs are used, which significantly pollute the environment; and if the Zn layer is not completely removed, in a humid environment, the Zn layer and the Ni-P layer will form a potential difference, which will lead to the corrosion phenomenon of the coating [21].

The use of large quantities of corrosive or toxic chemicals poses many problems for environmental protection related to waste liquids [22–24], and the whole treatment process is dangerous for the operators [25]. Achieving environmentally friendly pretreatment is in line with the development trend of chemical plating. The electromagnetic induction activation heating process proposed in this paper (Figure 1) excludes the use of corrosive chemicals to remove the surface of the oxide film. In the case of the substrate surface, it helps to prepare a layer of strong bonding and uniform distribution of the activated nickel layer. The resulting nickel nanoparticles are the catalytic centre of the EPN chemical plating and ultimately provide the strong bonding of a nickel-plated layer [26–29]. In this paper, a new activation process is proposed, which not only makes the operation easier but also reduces the pollution to the environment, providing a new direction for the surface treatment of materials.

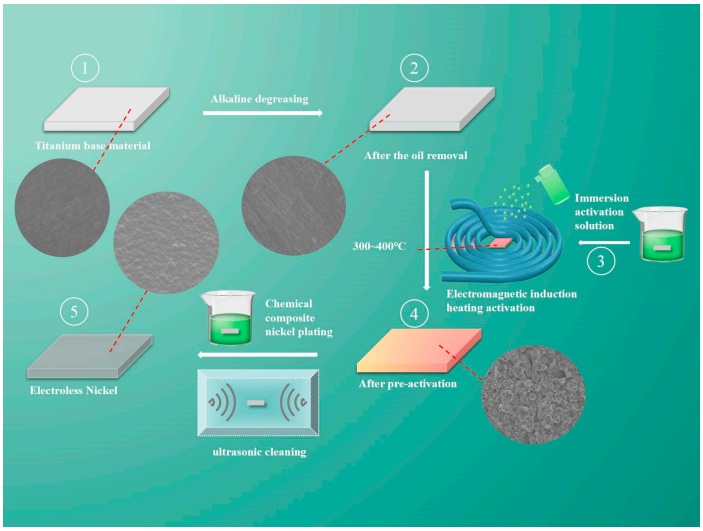


**Figure 1.** Flow chart of the electroless nickel plating process.

## 2. Materials and Methods

### *2.1. Materials*

Aluminium alloy plate was chosen as the substrate for the experimental material with a size of 3 mm × 10 mm × 30 mm. The main chemicals were NaOH, $Na_2CO_3$, $Na_3PO_4{\cdot}12H_2O$, $Ni_2SO_4{\cdot}6H_2O$, $NaH_2PO_2{\cdot}H_2O$, $CH_3COONa{\cdot}3H_2O$, $C_6H_5Na_3O_7{\cdot}2H_2O$, and complexing agent.

### *2.2. Degreasing of the Substrate*

The aluminium alloy was immersed in the degreasing solution (Table 1) and operated according to the conditions. Then, the treated substrate was placed in deionized water for ultrasonic cleaning for 5 min.

**Table 1.** Degreasing formulations.

| Formula | Reagent | Dosage | Concentration |
|---|---|---|---|
| I | $C_2H_6O$ | Just soak | 10 min ultrasonic washing |
| II | NaOH + $Na_2CO_3$ + $Na_3PO_4{\cdot}12H_2O$ | 25 g/L + 40 g/L + 40 g/L | Heat in a water bath at 50 °C and soak for 15 min. |
| III | Acetone aqueous solution | V($CH_3COCH$):V($H_2O$) = 1:1 | 30 min |

### *2.3. Surface Activation*

The ultrasonically treated substrate was immersed in the activation solution for 15~30 min and the substrate was removed and placed horizontally into the induction heating coil. High-frequency changes in the magnetic field inside the metal were used to generate eddy currents, and the internal free electrons' high-speed friction was used to generate heat—the experimental principle is shown in Figure 2. A digital thermometer (DM6801B) was used to measure the surface temperature of the specimen in real time. When the surface temperature reached 300~400 °C, the activation solution (Table 2) was sprayed uniformly on the surface of the specimen using an atomiser at a distance of about 30 cm and at a spray rate of 0.15–0.25 L/min, and then the activated substrate was placed into deionised water for ultrasonic cleaning, so that a layer of catalytically active nickel microparticles could be obtained on the surface of the activated substrate [30–32]. Important parameters of the non-destructive activation process were optimised using the L9 Taguchi method. The heating temperature of the substrate, the ionic concentration of the activation solution, and the spray rate ratio, which have a large influence on the activation process, were taken as factors, and the coverage of the revitalization layer was used as an evaluation indicator. The activated layer coverage (in $mm^2$) was calculated with Equation (1), and the process was optimised according to the 9 ($3^4$) orthogonal test scheme—Table 3 presents the orthogonal experiments.

$$X = \frac{N_1}{N_2} \times 100\% \quad (1)$$

where $X$ is the coverage rate, $N_1$ is the area covered by the activation layer, and $N_2$ is the area sprayed by the atomization of the activation liquid.

**Table 2.** Activating fluid formulations.

| Reagent | Concentration |
|---|---|
| $NiSO_4{\cdot}6H_2O$ | 10 g/L |
| $NaH_2PO_2{\cdot}H_2O$ | 60 g/L |

**Table 3.** Factors and levels of orthogonal experiment.

| Level | Element A | Element B | Element C |
|---|---|---|---|
| | Temperature/°C | $Ni^{2+}$:$H_2PO_2^-$ | Spray Rate/(L/min) |
| 1 | 200 | 1:4 | 0.15 |
| 2 | 300 | 1:5 | 0.2 |
| 3 | 400 | 1:6 | 0.25 |

Note: Levels of the factors are taken from the one-way test.

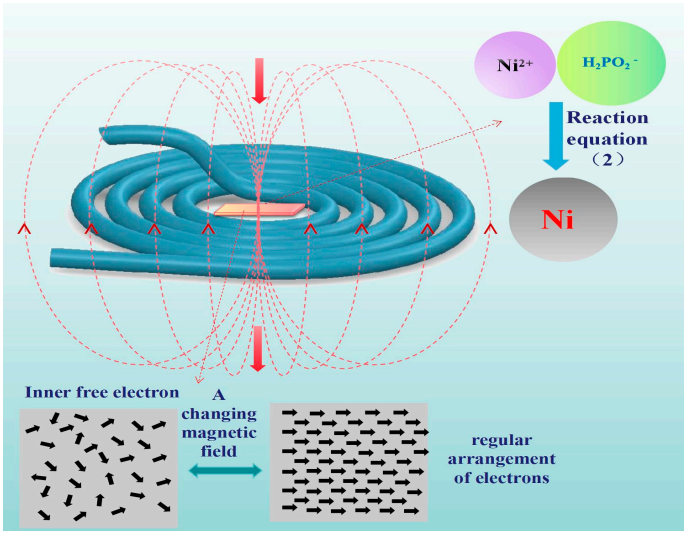


**Figure 2.** Experimental schematic diagram.

### *2.4. Electroless Nickel Plating*

The activated samples were immersed in the plating solution (Table 4) at 80 °C for 30–60 min.

**Table 4.** Plating solution formulation.

| Reagent | Concentration |
|---|---|
| $NiSO_4 \cdot 6H_2O$ | 25~30 g/L |
| $NaH_2PO_2 \cdot H_2O$ | 20~40 g/L |
| $CH_3COONa \cdot 3H_2O$ | 10~20 g/L |
| $C_6H_5Na_3O_7 \cdot 2H_2O$ | 25~30 g/L |
| $Al_2O_3$nanoparticle | 1.5~2.5 g/L |

### *2.5. Characterization*

The effect of degreasing is directly related to the final quality of the coating, so we used an optical angular contact meter (SDC-350H) to test the water contact angle of three degreasing formulas after degreasing and selected the optimal degreasing formula. The important parameters were optimised using the L9 Taguchi method, and then the data were analysed using Minitab 20 software.

The surface temperature of the specimen was measured with a digital thermometer (DM6801B). A scanning electron microscope (SEM) was used to observe the surface morphology before and after activation and the composite plating layer. Energy spectrum analysis of the activated and plated layers was carried out using energy dispersive spectroscopy (EDS). The elemental state of the activated layer surface was analysed by X-ray electron spectroscopy (XPS). The physical phase of the activated layer was analysed using an X-ray diffractometer (Empyrean, PANalytical).

The thermal shock method (ASTMB571) was used to test the samples. The experimentally obtained chemical nickel-plated specimens were put into the oven at 200 °C for 60 min

after heating and were then put into room temperature water to cool sharply; the cycle was 5 times, and the plating layer on the surface was not cracked or peeled off, indicating that the plating layer had good bonding force.

The equipment used in the experiment was a homemade device; the power of the device's operating voltage was 12–48 V, its maximum operating voltage was 48 V, its maximum operating power was 1000 W, its maximum operating current was 20 A, and its coil diameter was 10 cm.

## 3. Results and Discussion

### *3.1. Optimisation of Substrate Degreasing Parameters*

Figure 3a shows the hydrophilicity test results of the substrate before de-oiling—the water contact angle is 95.47°, the shape of the water droplets is round, the cohesion of water droplets is good, and there is no diffusion phenomenon. This indicates that a waterproof oil film is attached to the surface of the substrate, which will affect the adsorption of activation particles on the substrate during immersion, and will also affect the activation effect and the bonding force of the plating layer. Figure 3b–d shows the hydrophilicity test results of the substrate surface after de-oiling with anhydrous ethanol, a mixed solution of sodium hydroxide + sodium bicarbonate + sodium phosphate, and an aqueous acetone solution, respectively. It can be seen that the water contact angle is not the same after using different oil-removing liquids: the water contact angle of Formula I decreased to 75.90°; Formula II decreased to 55.11°; and Formula III decreased to 67.65°. It was found that Formula II had an obvious oil-removing effect, and the shape of the water droplets was flat, among which alkaline oil-removing liquids prepared with sodium hydroxide, sodium bicarbonate, and sodium phosphate in a certain proportion showed the best oil-removing effect. The alkaline degreasing liquid formulated with sodium hydroxide, sodium bicarbonate, and sodium phosphate in a certain proportion has the best degreasing effect.

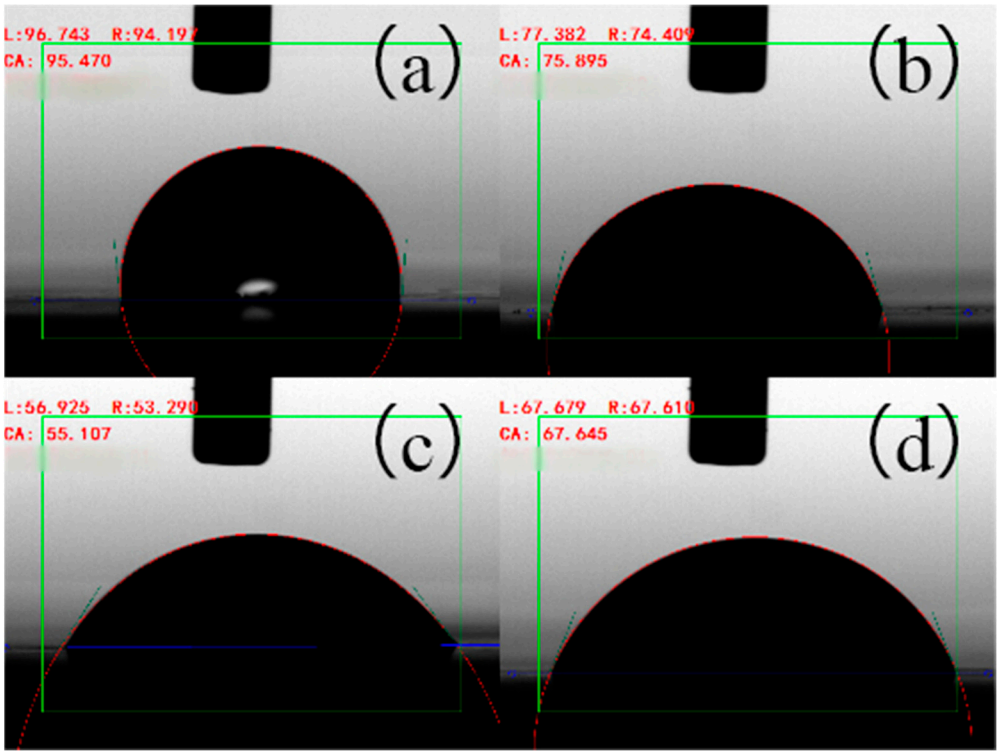


**Figure 3.** (**a**) Original; (**b**) Formulation I degreasing; (**c**) Formulation II degreasing; (**d**) Formulation III degreasing.

### 3.2. Optimization of Activation Parameters

The results of the orthogonal tests for the optimisation of the activation parameters are shown in Table 5. The results of the polar deviation show that the influence of each factor on the coverage of the activation layer is in the order of A > B > C. The optimal combination is A2B3C3, and therefore the optimal process conditions for activation are the addition of the heat temperature of about 300 °C, the ratio of the ionic concentration of $Ni^{2+}$:$H_2PO_2^-$ = 1:6, and the spraying rate of 0.25 L/min.

**Table 5.** Orthogonal test result and range analysis.

| No. | A | B | C | X/(mm$^2$) |
|---|---|---|---|---|
| 1 | 200 | 1:4 | 0.15 | 72 |
| 2 | 200 | 1:5 | 0.2 | 76.5 |
| 3 | 200 | 1:6 | 0.25 | 80.5 |
| 4 | 300 | 1:4 | 0.2 | 89.5 |
| 5 | 300 | 1:5 | 0.25 | 100 |
| 6 | 300 | 1:6 | 0.15 | 100 |
| 7 | 400 | 1:4 | 0.25 | 85.5 |
| 8 | 400 | 1:5 | 0.15 | 88.5 |
| 9 | 400 | 1:6 | 0.2 | 95 |
| averagesK1 | 76.333 | 82.333 | 86.833 | |
| averagesK2 | 96.500 | 88.333 | 87.000 | |
| averagesK3 | 89.667 | 91.833 | 88.667 | |
| | 20.167 | 9.500 | 1.834 | |

Analysing the mean value of the heating temperature of the substrate shows that K2 is slightly larger than K3 and much larger than K1, indicating that K2 is a better level, so A2 is chosen as the optimal heating temperature. The activation process then uses high temperature to provide energy to complete the reaction Equation (2).

$$Ni^{2+} + 4H_2PO_2^- + H_2O \rightarrow Ni + P + 3H_2PO_3^- + H^+ + \frac{3}{2}H_2 \uparrow \quad (2)$$

$$4NaH_2PO_2 \rightarrow Na_4P_2O_7 + 2PH_3 + H_2O \quad (3)$$

When the temperature of the surface of the control substrate reaches about 200 °C, the surface of the substrate begins to react, but the surface reaction area is small, and it cannot completely cover the surface of the substrate. When the temperature reaches between 300 and 400 °C, the nano-film generated on the surface of the substrate is able to completely cover it; when the temperature is higher than 400 °C, the surface of the substrate appears to be a black condensate block, the colour of the surface is changed, and there is no metallic lustre.

In reaction Equation (2), starting the reaction requires a temperature of only 200 °C, but in operation, the activation liquid spray will make the substrate surface temperature decrease, so the heating temperature should be higher than 200 °C. If the temperature is too high, sodium hypophosphite will be thermally decomposed to generate sodium pyrophosphate [33], which leads to a reduction of the reducing agent, reducing the reduction efficiency. Therefore, the temperature being too high will also have an effect. This inference is consistent with the obtained orthogonal, so the optimal heating temperature is about 300 °C.

Analysis of the ion concentration ratio to the mean value shows that too low a concentration of ions leads to insufficient coverage of the activation layer, while too high a concentration leads to the thermal decomposition of sodium hypophosphite to sodium pyrophosphate at high temperatures, as shown in reaction Equation (3).

Analysis of the average value of the spray rate revealed that if the spray rate is too low it will lead to the activation of the liquid on the surface of the substrate that is evaporated; if the rate is too high, it will lead to the activation of the liquid on the surface of the substrate

build-up, high-temperature conditions, and boiling bubbles, meaning that the activation of the layer is not complete.

### *3.3. Activation Analysis*

#### 3.3.1. Analysis of Activation Parameters

In the activation process, three main activation factors are considered (heating temperature, ion concentration ratio, spray rate), and different activation parameters will lead to a different quality of the activation layer. As shown in Figure 4a, activation under the conditions of slow spray rate, low ion concentration, and moderate temperature resulted in the activation layer not completely covering the surface of the substrate, which is due to the following reasons: the activation solution is evaporated by the high temperature in the process of spraying, resulting in the activation solution falling on the surface of the substrate less. The ion concentration ratio is insufficient, which leads to the nickel particles on the surface of the substrate reducing, resulting in the substrate not being completely covered and the activation effect being worse. As shown in Figure 4b, under the condition of a moderate spray rate, the activation layer will have a different quality if the different activation parameters are used. With a moderate spray rate, moderate ion concentration, moderate temperature conditions of activation, the activation of the activation layer of nickel particles is distributed uniformly and continuously. The reason for this is that the moderate spray rate can allow the appropriate amount of activation solution to fall to the surface of the substrate and the ion concentration ratio to meet the reaction equation; the temperature being moderate can also provide energy for the reactive reaction. As Figure 4c shows, in the conditions of activation, resulting in a large area of activation layer cover, there are cracks. The reason for this is that the activation solution is evaporated by the high temperature, the ion concentration is low, leading to nickel particles between the gap being large, and the bonding force is not strong. As shown in Figure 4d, if the spray rate is fast, the ion concentration is high, and the temperature is moderate under the condition of activation, the surface of the substrate nano-particle stacking is too much, which will affect the subsequent application of the plating, resulting in a decline in the quality of the plating layer.

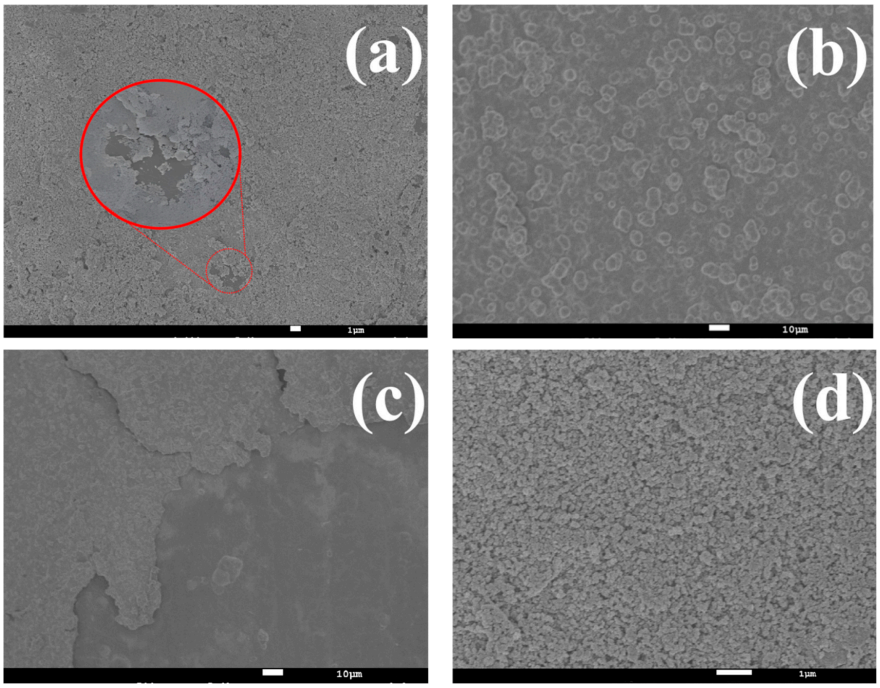


**Figure 4.** SEM of activated specimens with different parameters: (**a**) 0.15 L/min, $Ni^{2+}$:$H_2PO_2^-$ = 1:4, 310 °C; (**b**) 0.20 L/min, $Ni^{2+}$:$H_2PO_2^-$ = 1:5, 310 °C; (**c**) 0.15 L/min, $Ni^{2+}$:$H_2PO_2^-$ = 1:4, 450 °C; (**d**) 0.25 L/min, $Ni^{2+}$:$H_2PO_2^-$ = 1:6, 310 °C.

3.3.2. Optimal Activation Layer Analysis

The surface morphology of the activated substrate under the optimal activation conditions was analysed using scanning electron microscopy, as shown in Figure 5, where (a) and (b) show the surface morphology of the substrate before and after ultrasonic cleaning after activation, respectively. In Figure 5a, a large number of nanoparticles with a diameter of about 100 nm can be observed attached to the substrate surface, and the nanoparticles are in a stacked state. After ultrasonic cleaning, in Figure 5b, it can be observed that the nanoparticle stacking state disappears, and the surface is still attached with uniformly distributed nanoparticles, thus indicating that the activation process is able to prepare a layer of activated nanoparticles with a strong bonding force on the aluminium alloy surface. The changes in the elemental content of the sample surface before and after cleaning were analysed using EDS spectroscopy, as shown in Figure 5c,d. Comparing the EDS spectra before and after cleaning, it can be seen that the mass fractions of the elements did not change greatly after ultrasonic cleaning, and from the scanning data, it can be seen that the surface of the substrate contains O, Al, Ni, and P, which are uniformly distributed. Combined with the analysis of the SEM and EDS results mentioned above, it can be seen that the activation process can prepare a layer of nickel nanoparticles with a strong bonding force on the surface of aluminium alloy.

To further verify the experimental conclusions, the activated aluminium alloy surface was examined using XPS. As shown in Figure 6, the comparison of the fitted full spectrum (Figure 6a) shows that there are orbital peaks of Ni2p before and after ultrasonic cleaning, which proves that the activated layer has a strong binding force. The orbital peaks of Ni2p, P2p, O1s, and C1s appeared on the surface of the substrate after ultrasonic cleaning, respectively. In the Ni spectra shown in Figure 6b, there are two main peaks at 852.8 eV and 870.3 eV, which correspond to the 2p3/2 and 2p1/2 energy levels of Ni, respectively, indicating that there is a metallic nickel attached to the surface of the activated substrate. In summary, this indicates that the new activation process can produce a layer of catalytically active metallic nickel on the surface of the substrate [34].

3.3.3. Phase Structure of the Activated Layer

Figure 7 shows the XRD patterns of the aluminium alloy before and after the comparison of activated ultrasonic cleaning, from which it can be seen that before ultrasonic cleaning, three strong peaks can be observed at 2θ about 44.5°, 51.8°, and 76.4°, which are the crystallographic diffraction peaks of (111), (200), and (220) of Ni, respectively (PDF#87-7012). After ultrasonic cleaning, not only were the diffraction peaks of Ni detected but also the diffraction peaks of Al at 2θ about 38.5°, 44.7°, 65.1°, 78.2°, and 82.4°. However, the diffraction peaks of Al were masked by the diffraction peaks of Ni, indicating that the activation layer on the surface of the aluminium alloy before and after ultrasonication had no obvious change, and the bonding force was strong. From the space group, it can be seen that the nickel particles in the activation layer have a face-centred cubic crystal structure, and the peaks have sharp peak shapes, indicating that the product crystallization is complete and also indicating that the process does not change the crystal structure.

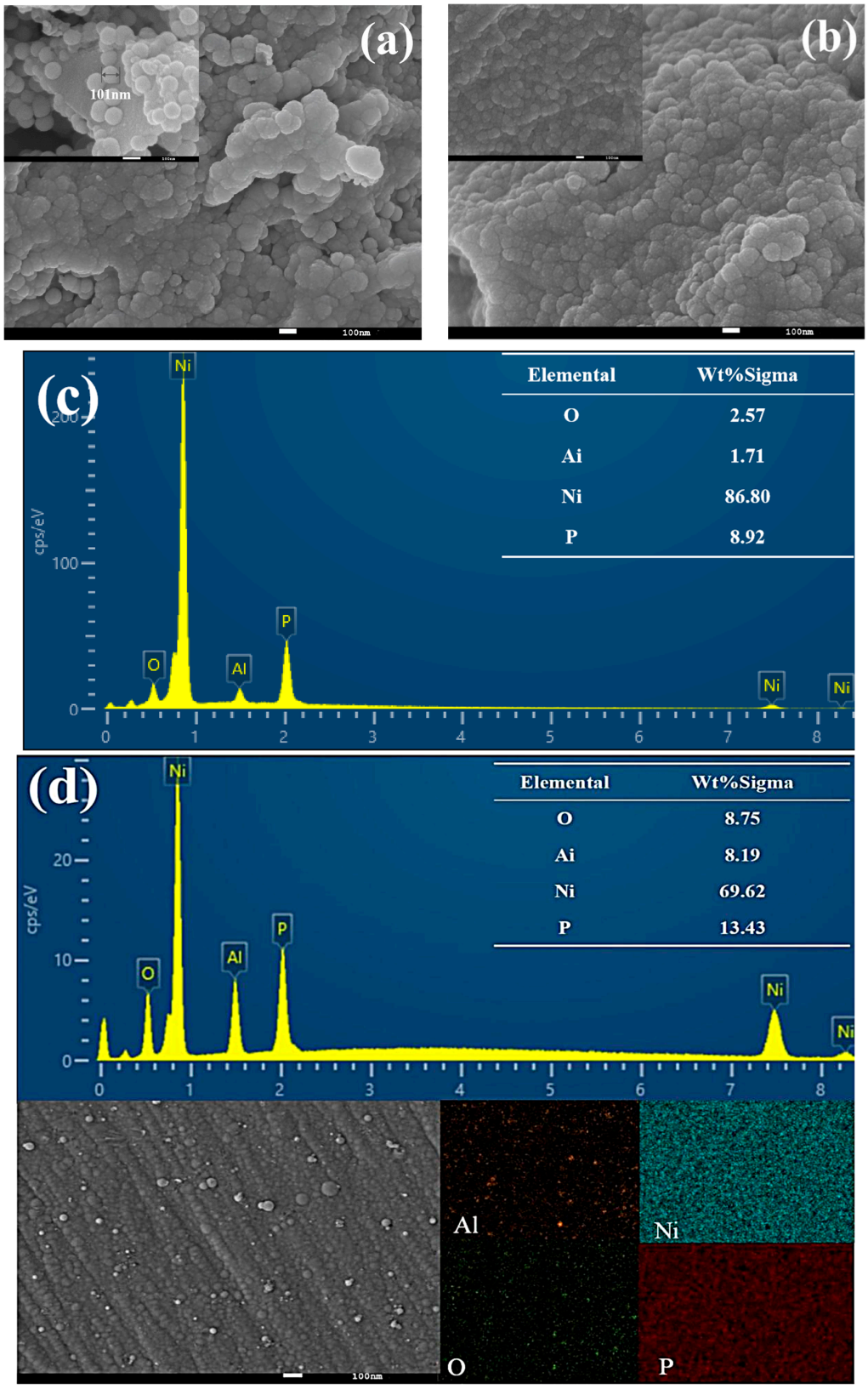


**Figure 5.** (**a**) SEM before ultrasonic cleaning; (**b**) SEM after ultrasonic cleaning. (**c**) EDS of the sample surface before cleaning; (**d**) EDS of the sample surface after cleaning.

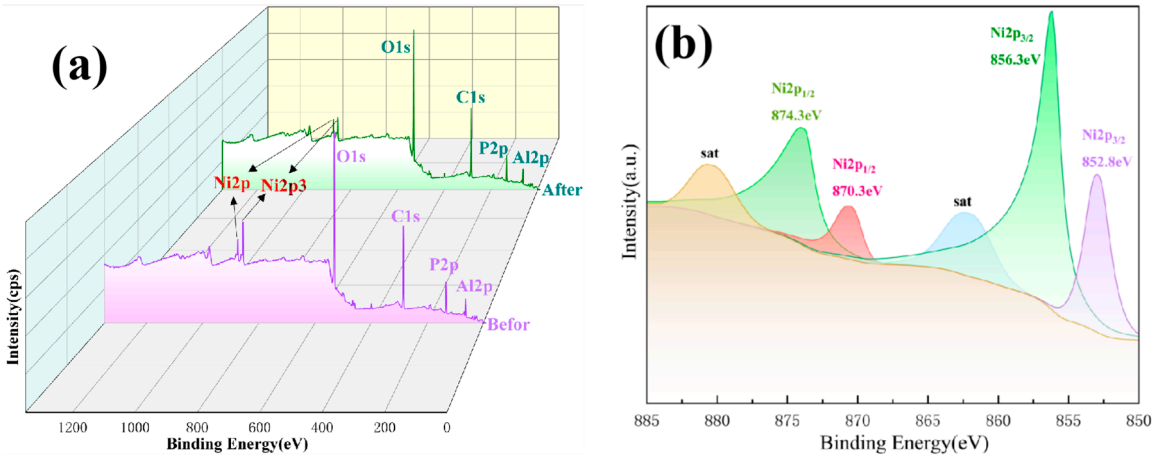


**Figure 6.** (**a**) Comparative analysis of the full spectrum of activated samples before and after ultrasonic cleaning; (**b**) Ni spectrum after sonication.

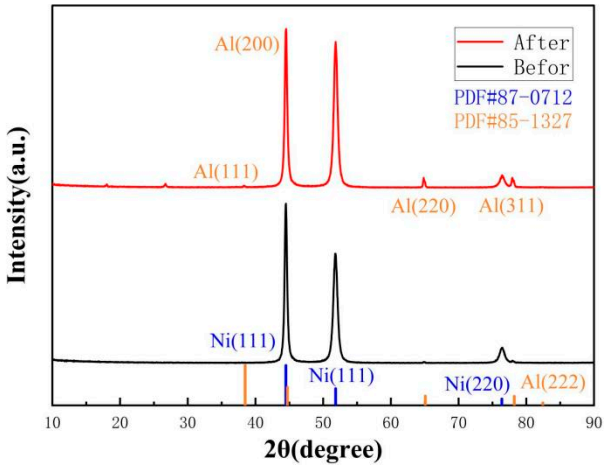


**Figure 7.** Substrate activation XRD.

### *3.4. ENP Analysis*

The total reaction equation of ENP is shown in (4):

$$NiL_m^{2+} + 4H_2PO_2^- + H_2O \rightarrow Ni + P + 3H_2PO_3^- + H^+ + \frac{3}{2}H_2 \uparrow + mL \quad (4)$$

L and m denote the ligand and coordination number, respectively, and the main function of the ligand is to prevent the experimental reaction from being intense and inhibit the generation of $Ni(OH)_2$, so the whole reaction can be simplified as reaction (1). The substrate is immersed and then put into the electromagnetic induction heating coil to be heated, and at the same time, the activation liquid is sprayed on the surface of the substrate by using the atomization device to catalyse the reaction (1) by using the temperature of the surface of the substrate to generate catalytic nickel nano-particles on the surface of the substrate, which has catalytic activity, because the electromagnetic induction heating process has the same effect as quenching. At the same time, the activation liquid sprayed on the surface temperature of the substrate is reduced, but the heat source is generated from the substrate. The heat source is generated from inside the substrate, so the activation solution on the surface of the substrate will rapidly shrink and generate nickel particles with a strong bonding force, and the whole process has the same effect as high-temperature welding. The plating process uses the nickel particles generated after activation as a catalytic centre for chemical plating, generating a continuous and uniform nickel layer on the surface of the substrate.

After 30 min of chemical nickel plating, the plating was subjected to a thermal shock test with ASTMB571 as the standard. The surface of the sample was smooth without defects and was flooded with nickel metal lustre before the thermal shock test, and the surface of the plating was not cracked or peeled off after the thermal shock test as shown in Figure 8a, which indicated that the plating bonding was good and complied with the standard of the plating. Figure 8b shows the samples prepared by the zinc dipping process at the same experimental temperature as well as the plating application time. After passing the thermal shock test, the surface is similar to that of the samples prepared by the new process without any significant change, indicating that the bonding strength of the plated layers prepared by both processes is very good.




**Figure 8.** Specimen after thermal shock test: new process (**a**); Zinc dipping process (**b**).

## 4. Conclusions

1. In this research, a new process of non-destructive chemical plating of Ni-P on an aluminium alloy surface with electromagnetic induction heating activation is proposed. This new process does not damage the substrate and is environmentally friendly. It not only avoids damaging the substrate's surface during roughening but also simplifies the operation process and saves a lot of time compared with the commonly used zinc dipping process. This study provides a new direction for the surface treatment of aluminium alloys and is simpler and more environmentally friendly than the commonly used processes.

2. This process can effectively generate a layer of catalytically active nickel nanoparticles on the surface of aluminium alloy with a strong bonding force. ENP uses nickel nanoparticles as the catalytic centre to generate a uniform and continuous nickel metal covering the entire surface of the substrate. The final coating obtained after the thermal shock test can still maintain the coating without significant changes, indicating that the prepared coating has a strong binding force and meets the standard. To summarize, the new process proposed in this paper is simple in operation, low cost, environmentally friendly, and has important industrial potential.

**Author Contributions:** Conceptualization, J.G., K.C. and S.L.; methodology, J.G. and K.C.; validation, S.L., R.Q. and K.C.; formal analysis, L.Z. and J.D.; investigation, J.G., Z.Y. and S.L.; data curation, J.G. and S.L.; writing—original draft preparation, J.G. and S.L.; writing—review and editing, J.G., S.L. and K.C.; visualization, J.G., R.Q. and S.L.; supervision, L.Z., Z.Y., J.D. and K.C.; project administration, R.Q., Z.Y. and K.C.; funding acquisition, L.Z., J.G. and S.L. All authors have read and agreed to the published version of the manuscript.

**Funding:** This work was supported by the Science and Technology Department of Sichuan Province, China [grant number 23ZS2127]; the Science and Technology Department of Sichuan Province, China [grant numbers 20ZS2112]; the Sichuan Science and Technology Innovation Talent Project, China

[grant number 2022JDRC0028]; the Research Foundation of Southwest University of Science and Technology, China [grant number 19zx7165].

**Institutional Review Board Statement:** Not applicable.

**Informed Consent Statement:** Not applicable.

**Data Availability Statement:** Data are contained within the article.

**Conflicts of Interest:** The authors declare no conflicts of interest.

## References

1. Selivanov, A.A.; Tkachenko, E.A.; Oglodkova, Y.S.; Benarieb, I. Trends in the development of aluminum alloys for power elements of aviation engineering components within Russia and abroad. *Rev. Metall.* **2024**, *67*, 1845–1855. [CrossRef]
2. Jafari-Tarzanagh, Y.; Seifzadeh, D.; Khodayari, A.; Samadianfard, R. Active corrosion protection of AA2024 aluminum alloy by a sol-gel coating containing inhibitor-loaded mesoporous SBA-15. *Prog. Org. Coat.* **2022**, *173*, 107166. [CrossRef]
3. Tarzanagh, Y.J.; Seifzadeh, D.; Rajabalizadeh, Z.; Habibi-Yangjeh, A.; Khodayari, A.; Sohrabnezhad, S. Sol-gel/MOF nanocomposite for effective protection of 2024 aluminum alloy against corrosion. *Surf. Coat. Technol.* **2019**, *380*, 125038. [CrossRef]
4. Chang, L.M.; Wang, P.; Liu, W. Effect of amino acids on the structure and corrosion resistance of Mg-Li alloy anodic oxide film. *Adv. Mater. Res.* **2011**, *146*, 785–788. [CrossRef]
5. Zhang, H.; Yao, G.C.; Wang, S.L.; Liu, Y.H.; Luo, H.J. A chrome-free conversion coating for magnesium-lithium alloy by a phosphate–permanganate solution. *Surf. Coat. Technol.* **2008**, *202*, 1825–1830. [CrossRef]
6. Zou, Y.; Zhang, Z.W.; Liu, S.Y.; Chen, D.; Wang, G.X.; Wang, Y.Y.; Zhang, M.L.; Chen, Y.H. Ultrasonic-Assisted Electroless Ni-PPlating on Dual Phase Mg-Li Alloy. *J. Electrochem. Soc.* **2014**, *162*, C64–C70. [CrossRef]
7. Zhang, J.; Duan, X.; Hou, A.; Li, J.; Wang, K.; Cai, H. In Situ Preparation of Mg-Al-Co Layered Double Hydroxides on MicroarcOxidation Ceramic Coating of LA103ZMagnesium-Lithium Alloy for Enhanced Corrosion Resistance. *J. Mater. Eng. Perform.* **2021**, *30*, 8490–8499. [CrossRef]
8. Radwan, A.B.; Ali, K.; Shakoor, R.; Mohammed, H.; Alsalama, T.; Kahraman, R.; Yusuf, M.M.; Abdullah, A.M.; Montemor, M.F.; Helal, M. Properties enhancement of Ni-P electrodeposited coatings by the incorporation of nanoscale Y2O3 particles. *Appl. Surf. Sci.* **2018**, *457*, 956–967. [CrossRef]
9. Jiang, Z.; Xu, X.; Cheng, H.; Liu, Q.J.; Zhang, X.; Zhou, K.X.; Huang, J. Effect of submicron Sn and heat treatment temperature on corrosion resistance of Ni-P composite coatings. *Mater. Res. Express* **2019**, *6*, 076573. [CrossRef]
10. Elahinejad, S.; Sharifi, H.; Tayebi, M.; Rajaee, A. The influence of nickel coating on the interface of pressureless infiltrated with vibration Al–SiC composites. *Mater. Res. Express* **2017**, *4*, 116506. [CrossRef]
11. Omar, R.; Aboraia, M.S.; A Oraby, E.; Gubner, R.; Rizk, A.E. The effect of sodium citrate as a complex agent on the corrosion properties of the electroless Ni-P coating. *Mater. Res. Express* **2018**, *5*, 126511. [CrossRef]
12. Shi, Q.-Y.; Liu, Z.-Q.; Wu, D.; Zhang, H.; Ni, D.-R.; Suganuma, K. Fabrication of Ni–P coating film on diamond/Al composite and its soldering reliability. *J. Mater. Sci. Mater. Electron.* **2018**, *29*, 8371–8379. [CrossRef]
13. Fetohi, A.E.; Hameed, R.M.A.; El-Khatib, K.M. Development of electroless Ni–P modified aluminum substrates in a simulated fuel cell environment. *J. Ind. Eng. Chem.* **2015**, *30*, 239–248. [CrossRef]
14. Romero-Romero, M.; Domínguez-Ríos, C.; Torres-Sánchez, R.; Aguilar-Elguezabal, A. Electroless Ni-Bcoating onto TiH2 powder: An approach for a simplified surface preparation. *J. Surf. Coat. Technol.* **2017**, *315*, 181–187. [CrossRef]
15. Zhao, Q.; Hu, G.; Huang, R.; Qiang, L.; Zhang, X. Iodide-induced galvanic replacement of nickel film on copper as an activator for electroless nickel-phosphorus plating. *Mater. Lett.* **2022**, *314*, 131833. [CrossRef]
16. Gutiérrez, A.G.G.; Pech-Canul, M.A.; Sebastian, P.J. Zincating effect on corrosion resistance of electroless Ni-P coating on aluminum alloy 6061. *Fuel Cells* **2017**, *17*, 770–777. [CrossRef]
17. Rajabalizadeh, Z.; Seifzadeh, D.; Habibi-Yangjeh, A.; Gundoshmian, T.M.; Nezamdoust, S. Electrochemical noise analysis to examine the corrosion behavior of Ni-P deposit on AM60B alloy plated by Zr pretreatment. *Surf. Coat. Technol.* **2018**, *346*, 29–39. [CrossRef]
18. Yazdi, S.S.; Ashrafizadeh, F.; Hakimizad, A. Improving the grain structure and adhesion of Ni-P coating to 3004 aluminum substrate by nanostructured anodic film interlayer. *Surf. Coat. Technol.* **2013**, *232*, 561–566. [CrossRef]
19. Fetohi, A.E.; Hameed, R.A.; El-Khatib, K. Ni–P and Ni–Mo–P modified aluminum alloy 6061 as bipolar plate material for proton exchange membrane fuel cells. *J. Power Sources* **2013**, *240*, 589–597. [CrossRef]
20. Qi, Z.; Lu, W.; Guo, A.; Hu, Y.; Lee, W.; Zhang, X. Investigation on Circular Plating Pit of Electroless Ni–P Coating. *Ind. Eng. Chem. Res.* **2014**, *53*, 3097–3104. [CrossRef]
21. Gayo, G.X.; Lavat, A.E. Green ceramic pigment based on chromium recovered from a plating waste. *J. Ceram. Int.* **2018**, *44*, 22181–22188. [CrossRef]
22. Padhan, R.K.; Gupta, A.; Badoni, R.; Bhatnagar, A. Poly(ethylene terephthalate) waste derived chemicals as an antistripping additive for bitumen–An environment-friendly approach for disposal of environmentally hazardous material. *J. Polym. Degrad. Stab.* **2013**, *98*, 2592–2601. [CrossRef]

23. Rodríguez, R.; Espada, J.; Gallardo, M.; Molina, R.; López-Muñoz, M. Life cycle assessment and techno-economic evaluation of alternatives for the treatment of wastewater in a chrome-plating industry. *J. Clean. Prod.* **2018**, *172*, 2351–2362. [CrossRef]
24. Suman, R.; Nandan, D.; Haleem, A.; Bahl, S.; Javaid, M. Experimental study of electroless plating on acrylonitrile butadiene styrene polymer for obtaining new eco-friendly chromium-free processes. *J. Mater. Today.: Proc.* **2020**, *28*, 1575–1579. [CrossRef]
25. Askri, F.; Mellouli, S.; Alqahtani, T.; Algarni, S.; Alshammari, B.M.; Kolsi, L. Performance improvement of metal hydride hydrogen compressors using electromagnetic induction heating. *Alex. Eng. J.* **2024**, *98*, 103–113. [CrossRef]
26. Guan, D.; Wang, F.; Zhang, X.; Dou, W.; Sun, Y. Comprehensive study on catalytic coating tubular reactor with electromagnetic induction heating for hydrogen production through methanol steam reforming. *Int. J. Hydrog. Energy* **2024**, *50*, 1–17. [CrossRef]
27. Cervera-Gabalda, L.; Gómez-Polo, C. Magnetic carbon Fe3O4 nanocomposites synthesized via Magnetic Induction Heating. *Sci. Rep.* **2023**, *13*, 7244. [CrossRef]
28. Dang, X.; Cui, K.; Zhuang, J.; Zhong, L.; He, Y.; Li, G.; Du, G.; Yang, Z.; Pei, S.; Li, S. A new process for environmentally friendly and non-destructive activation of electroless nickel plating on alumina ceramics. *J. Mater. Today Commun.* **2023**, *35*, 105506. [CrossRef]
29. Li, L.; An, M. Electroless nickel-phosphorus plating on SiCp/Al composite from acid bath with nickel activation. *J. Alloys Compd.* **2008**, *461*, 85–91. [CrossRef]
30. Yung, M.M.; Starace, A.K.; Mukarakate, C.; Crow, A.M.; Leshnov, M.A.; Magrini, K.A. Biomass catalytic pyrolysis on Ni/ZSM-5: Effects of nickel pretreatment and loading. *Energy Fuels* **2016**, *30*, 5259–5268. [CrossRef]
31. Dai, K.J.; Xiong, Y.; Zhang, X.L. Preparation of electroless Ni–P coating on ZnS substrate by strike nickel activation process. *Mater. Technol.* **2014**, *29*, 241–244. [CrossRef]
32. Kang, R.; An, M.; Cui, F.; Wang, J.; Liang, J. Galvanic deposition of Ni on Al alloy from a choline chloride-based ionic liquid for electroless Ni–P pretreatment. *Mater. Res. Express* **2019**, *6*, 1165a6. [CrossRef]
33. Liu, D.; Li, X.; Wei, L.; Zhang, T.; Wang, A.; Liu, C.; Prins, R. Disproportionation of hypophosphite and phosphite. *J. Dalton Trans.* **2017**, *46*, 6366–6378. [CrossRef] [PubMed]
34. Zhang, P.; Lv, Z.; Liu, X.; Xie, G.; Zhang, B. Electroless nickel plating on alumina ceramic activated by metallic nickel as electrocatalyst for oxygen evolution reaction. *J. Catal. Commun.* **2021**, *149*, 106238. [CrossRef]


**Disclaimer/Publisher's Note:** The statements, opinions and data contained in all publications are solely those of the individual author(s) and contributor(s) and not of MDPI and/or the editor(s). MDPI and/or the editor(s) disclaim responsibility for any injury to people or property resulting from any ideas, methods, instructions or products referred to in the content.